Biomedical Sciences and Clinical Medicine 2023;62(4):169-180.
doi: 10.12982/BSCM.2023.17
https://heo1.tci-thaijo.org/index.php/CMMJ-MedCMJ/index

BSCM
Biomedical Sciences and Clinical Medicine

Original Article **Open Access**

Multi-Target Actions of Flavonoid Derivatives from *Mesua ferrea* Linn Flower against Alzheimer's disease Pathogenesis

Kusawadee Plekratoke[1], Pornthip Waiwut[2], Chavi Yenjai[3], Orawan Monthakantirat[4], Pitchayakarn Takomthong[4], Natsajee Nualkaew[4], Suresh Awale[5], Yaowared Chulikhit[4], Supawadee Daodee[4], Charinya Khamphukdee[4] and Chantana Boonyarat[4]

[1]Biomedical Science Program, Graduate School, Khon Kaen University, Khon Kaen, [2]Faculty of Pharmaceutical Sciences, Ubon Ratchathani University, Ubon Ratchathani, [3]Department of Chemistry, Faculty of Science, Khon Kaen University, [4]Faculty of Pharmaceutical Sciences, Khon Kaen University, Khon Kaen, Thailand, [5]Natural Drug Discovery Lab, Institute of Natural Medicine, University of Toyama, Toyama, Japan

Correspondence:
Chantana Boonyarat, PhD,
Faculty of Pharmaceutical Sciences, Khon Kaen University, 123 Moo 16 Mitraphab Road , Muang, Khon Kaen 40002, Thailand.
e-mail: chaboo@kku.ac.th

Received: August 23, 2023;
Revised: October 16, 2023;
Accepted: October 30, 2023

ABSTRACT

OBJECTIVE Kaempferol-3-*O*-rhamnoside (compound 1) and quercetin-3-*O*-rhamnoside (compound 2), two flavonoids isolated from *Mesua ferrea* L. flowers, were examined for their activities related Alzheimer's disease (AD) pathogenesis including antioxidant, acetylcholinesterase (AChE) inhibition, anti-beta amyloid (Aβ) aggregation and neuroprotection.

METHODS The two flavonoids were isolated from *M. ferrea* L. flowers using the column chromatography technique. Both compounds were evaluated for their effects on AD pathogenesis, including antioxidant action by ABTS assay, AChE inhibition by Ellman's method, and anti-Aβ aggregation by thioflavin T (ThT) assay and neuroprotection by cell base assay. To explain the mechanism of AChE inhibition and anti-Aβ aggregation, binding interactions between the test compounds and AChE and Aβ were studied *in-silico*.

RESULTS Compounds 1 and 2 showed an ability to scavenge ABTS radicals, with IC_{50} values of 424.57±2.97 and 308.67±9.90 µM, respectively, and to inhibit AChE function with IC_{50} values of 769.23±6.23 and 520.64±5.94, respectively. ThT assay indicated that both compounds inhibited Aβ aggregation with IC_{50} values of 406.43±9.95 and 300.69 ±1.18 µM, respectively. The neuroprotection study revealed that the two flavonoids could reduce human neuroblastoma (SH-SY5Y) cell death induced by H_2O_2. The *in-silico* study showed that both compounds bound AChE at catalytic anionic and peripheral anionic sites. In addition, the test compounds prevented Aβ aggregation by interacting at the central hydrophobic core, the C-terminal hydrophobic region, and the important residues of Ile41.

CONCLUSIONS Together, the results showed that kaempferol-3-*O*-rhamnoside and quercetin-3-*O*- rhamnoside exhibit multiple mechanisms of action that are involved in the pathogenesis of AD including antioxidant, AChE inhibition, anti-Aβ aggregation, and neuroprotection.

KEYWORDS flavonoid rhamnosides, Alzheimer's disease, oxidation, beta amyloid, acetylcholinesterase, molecular docking

INTRODUCTION

The most common kind of dementia is Alzheimer's disease (AD), also known as senile dementia. The prevalence of AD gradually increases with age, reaching a maximum incidence rate of 50% in people over the age of 85 (1). The World Health Organization reported that AD affected more than 58 million individuals worldwide in 2021. According to estimates, there will be 88 million AD patients worldwide in 2050. The cost of treating and caring for AD patients worldwide was $957.56 billion in 2015, and it is estimated to rise to $2.54 trillion in 2030 and $9.12 trillion in 2050 (2, 3). The pathogenesis of AD has been found to be associated with many pathways, including aggregation of Aβ (4), formation of neurofibrillary tangles (5), lack of cholinergic neurotransmission (6), neuroinflammation (7), and oxidative stress (8). Currently, only five drugs (rivastigmine, galantamine, donepezil, memantine, and Namzaric®) have been approved by United States Food and Drug Administration (FDA) for the treatment of AD (9). However, these drugs, which are single target drugs, only help with palliative care; they have no effect on curing or preventing AD. Thus, compounds that can hit multiple targets linked to AD are still required.

Flavonoids, a major class of hydroxylated polyphenolic compounds found in vascular plants, have numerous benefits as food and medication. Flavonoids have the basic structure C6-C3-C6. Based on the position of ring B that ring C is connected to and the degree of ring C unsaturation, flavonoids can be classified into several subclasses such as flavanols, flavanones, flavones, flavanonols, isoflavones, and anthocyanidins (10). Currently, over 9,000 compounds with a flavonoid skeleton have been identified, some of which are coupled with sugars like glucose, xylose, arabinose, glucuronic acid and rhamnoside (11, 12). Flavonoids have been found to exhibit numerous biological activities and anti-AD effects including antioxidant, anti-AChE, anti-Aβ and anti-inflammatory (13).

A plant of the Calophyllaceae family called *Mesua ferrea* L. is widely scattered in tropical region like India, Thailand, and China. Several studies revealed that the extract of *M. ferrea* L. flower showed biological activities related to AD such as anti-inflammation (14), antioxidant (15), anti-Aβ aggregation, and AChE inhibitory action (16). A review of the literature found that kaempferol-3-*O*-rhamnoside, and quercetin-3-*O*-rhamnoside are the major compounds isolated from the flower of *M. ferrea* L. (17). Both kaempferol-3-*O*-rhamnoside, and quercetin-3-*O*-rhamnoside have various biological activities, e.g., anti-cancer (18), anti-diabetic (19), and antiviral (20). However, there are no reports of flavonol rhamnoside as being anti-AD. The objectives of this study were to isolate the flavonoid rhamnosides from *M. ferrea* L. flower and to assess their activities associated with AD including antioxidant, AChE function, Aβ aggregation, and neuroprotection. To clarify the mechanism of AChE inhibition and anti-Aβ aggregation, binding interactions between the flavonoid rhamnosides and AChE or Aβ were also studied *in-silico*.

METHODS

Materials

The powder of *M. ferrea* L. flower was obtained from Chao Phya Abhaibhubejhr Hospital, Prachinburi Province, Thailand. It was identified by Benjawan Leenin, leader of the Traditional Knowledge Center, Chao Phya Abhaibhubejhr Hospital Foundation. The herbarium voucher specimen of *M. ferrea* L. was deposited at the museum of Chao Phya Abhaibhubejhr Hospital with voucher number YPJ013. The reference compounds, i.e. trolox, tacrine, curcumin, N-acetyl cysteine (NAC) and other chemicals like 2,2'-azino-bis (3-ethylbenzthiazoline-6-sulphonic acid) (ABTS), acetylcholinesterase from *Electrophorus electricus* (electric eel), and Dulbecco's modified Eagle medium nutrient mixture F-12 (DMEM/F12), were purchased from Sigma-Aldrich (SM Chemical supplies Co., Ltd., Bangkok, Thailand). $A\beta_{1-42}$ was ordered from Abcam (Prima Scientific Co., Ltd., Bangkok, Thailand).

Extraction and isolation of flavonoids from *M. ferrea* L. flower extract

The powder of *M. ferrea* L. flower (3 kg) was extracted successively using hexane (3 × 4 L), EtOAc (3 × 4 L) and MeOH (3 × 4 L) at room

temperature. All the extracts were then evaporated using a rotary evaporator at 40-50 °C to obtain crude hexane (103 g), EtOAc (162 g), and MeOH (178 g) extracts. The MeOH extract was subjected to silica gel column chromatography (CC) and eluted with CH_2Cl_2 and MeOH using a gradient system to provide fractions F_1-F_9. Fraction F_6 (15 g) was purified by silica gel CC, eluted with a gradient system of CH_2Cl_2: MeOH (85:15→0:100, v/v) to give eight fractions, $F_{6.1}$-$F_{6.8}$. Fraction $F_{6.5}$ (3.2 g) was separated by CC using CH_2Cl_2: MeOH (95:5→0:100, v/v) to obtain nine subfractions, $F_{6.5.1}$-$F_{6.5.9}$. Subfraction $F_{6.5.8}$ was subjected to preparative thin-layer chromatography (PTLC) using CH_2Cl_2: MeOH (85:15) as the developing solvent to obtain compound 1 (229.1 mg). Fraction F_7 (13.3 g) was isolated by CC using silica gel, eluted with CH_2Cl_2: MeOH (85:15→0:100, v/v) to obtain eight fractions, $F_{7.1}$-$_{7.8}$. Fraction $F_{7.5}$ was subjected to reversed phase silica gel CC, eluted with a gradient system of H_2O_2, i.e., MeOH (2:1→1:1→0:1), to obtain five fractions, $F_{7.1}$-$F_{7.5}$. Fraction $F_{7.3}$ was subjected to Sephadex LH-20 CC and was eluted with 100% MeOH to obtain compound 2 (292.5 mg).

Identification of isolated compounds

For chemical structure elucidation, IR, 1H NMR, ^{13}C NMR, and MS, which are based on spectroscopic data, were used. IR spectra of the compounds 1 and 2 were recorded as KBr disks, using a Perkin Elmer Spectrum One FT-IR spectrophotometer. The 1H NMR and ^{13}C NMR spectra were recorded on a Varian Mercury plus spectrometer (Bruker, Model: Ascend-400) operating at 400 MHz and 100 MHz, respectively, using TMS as an internal standard. Liquid chromatography-high resolution electrospray ionization mass spectrometry (LC-HRESIMS) was used to accurately determine the mass of the isolated compounds.

***In vitro* analysis**

Antioxidant activity by ABTS assay

The effect of flavonoid rhamnosides on antioxidant activity was investigated using ABTS assay as described by Rajurkar et al. (21). Radical ABTS ($ABTS^{\cdot+}$) was generated by the oxidation of ABTS with potassium persulfate ($K_2S_2O_8$). A mixture of 7 mM ABTS and 2.45 mM $K_2S_2O_8$ (1:1; v/v) was incubated in the dark for 12-16 h and kept at room temperature. A total of 150 µL of reaction mixture containing 100 µL of $ABTS^{\cdot+}$ and 50 µL of a sample was added to a 96-well plate. The plate was incubated for 30 minutes at room temperature in the dark and the absorbance of the samples was detected at a wavelength of 700 nm. The results are reported as IC_{50} values. Trolox was used as the reference standard.

Acetylcholinesterase activity by Ellman's method

The Ellman's method was used to measure AChE activity using a microplate reader. The AChE enzyme hydrolyses the substrate acetylthiocholine (ATCI) resulting in the product thiocholine. Thiocholine interacts with 5,5′-dithiobis-(2-nitrobenzoic acid) (DTNB) to provide 2-nitrobenzoate-5-mercaptothiocholine and 5-thio-2-nitrobenzoate, which can be measured at 405 nm. For the experiment, 25 µL of 1 mM ATCI, 125 µL of 1 mM DTNB, 25µL of the sample, and 50 µL of 0.2 U/mL AChE from an electric eel (type VI-S) were added to the 96-wells. The absorbance was measured at 405 nm every 30 s for 5 minutes using a microplate reader. The results are expressed as IC_{50} values (22). Tacrine was used as the reference compound.

Aβ aggregation activity by Thioflavin T assay

The Thioflavin T (ThT) assay was used to evaluate the Aβ aggregates. $Aβ_{1-42}$ was dis-solved in pH 7.4 phosphate-buffered saline (PBS) and kept at -20 °C until use. To evaluate the effects on Aβ aggregation, 2 µL of the sample at various concentrations dissolved in DMSO was incubated with 18 µL of 10 µM $Aβ_{1-42}$ at 37 °C for 48 h in the dark. After 48 h, 180 µL of 5 µM ThT in a glycine/NaOH solution (pH 8) were added to the plate. Then, the fluorescence was measured after 5 minutes using a microplate reader with excitation at 446 nm and emission at 490 nm (23). Curcumin was used as a reference standard.

Neuroprotective analysis

The SH-SY5Y cells were cultured in a medium of DMEM/F12 supplemented with 10% FBS in a humidified 5% CO_2 incubator at 37 °C. To differentiate neural cells, the cells were cultured in a 75 cm^2 cell culture flask for 24 h. Then the cells were differentiated with 10 µM retinoic acid (RA) in 1% FBS in a culture medium for 6

days. Every three days, the media that contained RA were replaced (24). Before testing, the differentiated SH-SY5Y cells were cultured in 96-well plates at a concentration of 5 x 10^5 cells/mL and incubated for 48 h. After 48 h, the cells were pretreated either with the samples or the reference compound (n-acetylcysteine; NAC) for 2 h. For oxidative stress induction, cells were treated with 100 µl of 250 µM H_2O_2 for 2 h. Then the cells were stained with 100 µL of 0.5 mg/mL MTT for 2 h and identified using microplate reader at a wavelength of 550 nm (25).

In-silico binding interaction studies

The interaction between the targets and flavonoid rhamnosides was determined using molecular docking studies. AChE structure was obtained from the protein data bank (PDB: code: 2CEK). For the 3D optimization of the test compounds, Chem3D 15.1 was used. The AutoDock 4.2.6 program was used for the docking study. After the docking process, BIOVIA Dis covery Studio 2017 was used to analyze the interactions. For the Aβ fibril study, X-ray crystallography with PDB code 2BEG was used to create the template. The Autodock 4.2.6 program was used to perform the docking which was repeated for 100 runs using the Lamarckian genetic algorithm. The maximum number of generations and the energy evaluation of determination were set at 27,000 and 1,000,000, respectively. BIOVIA Discovery Studio 2017 was used to analyze the interactions (26).

Statistical analyses

For *in vitro*, the data are reported as means ±SD (n = 3-5). Statistical significance was determined by one-way analysis of variance (ANOVA). A p <0.05 was considered as statistically significant. The data were analyzed using IBM SPSS statistics 19.0 software.

RESULTS

Characterization of isolated compounds from *M. ferrea* L.

The MeOH extract of *M. ferrea* L. flower was isolated by column chromatography to obtain two flavonol rhamnoside compounds, kaempferol 3-*O*-rhamnoside (compound 1) and quercetin 3-*O*-rhamnoside (compound 2). For chemical structure elucidation, the spectrum data of compounds 1 and 2 were obtained from IR, ^{1}H NMR, ^{13}C NMR, and HRESIMS.

Compound 1. Kaempferol 3-*O*-rhamnoside, a yellow powder; IR $_{Vmax}$ 3391, 2978, 1656, 1361, 1177, and 839 cm^{-1}. ^{1}H NMR (CD_3OD, 400 MHz, δ_H) δ 7.76 (2H, dd, *J* = 8.8 Hz, H-2′ and H-6′), 6.92 (2H, dd, *J* = 8.4 Hz, H-3′ and H-5′), 6.34 (1H, d, *J* = 1.6 Hz, H-8), 6.17 (1H, d, *J* = 1.6 Hz, H-6), 5.36 (1H, d, *J* = 1.6 Hz, H-1″), 4.21 (1H, d, *J* = 1.2 Hz, H-2″), 3.70 (1H, dd, *J* = 3.2, 8.8 Hz, H-3″), 3.30 (2H, m, H-4″ and H-5″), and 0.91 (3H, d, *J* = 5.6 Hz, CH_3-6″). ^{13}C NMR (CD_3OD, 100 MHz, δ_C) 178.06 (C-4), 165.71 (C-7), 161.77 (C-5), 160.18 (C-2), 157.72 (C-4′), 157.25 (C-9), 134.70 (C-3), 130.42 (C-2′ and C-6′), 121.18 (C-1′), 115.13 (C-3′ and C-5′), 104.17 (C-10), 102.07 (C-1″), 98.77 (C-6), 93.62 (C-8), 71.78 (C-4″), 70.70 (C- 2″), 70.60 (C-3″), 70.50 (C-5″), 16.10 (CH3-6″). HRESIMS: m/z 455.0951 $[M+Na]^+$.

Compound 2. Quercetin 3-*O*-rhamnoside, a yellow powder; IR $_{Vmax}$ 3391, 2932, 1655, 1359, 1173, 814 cm^{-1}. ^{1}H NMR (CD_3OD, 400 MHz, δ_H) δ 7.32 (^{1}H, d, *J* = 2.0 Hz, H-2′), 7.30 (1H, dd, *J* = 8.0, 2.0 Hz, H-6′), 6.91 (1H, d, *J* = 8.4 Hz, H-5′), 6.38 (1H, d, *J* = 2.0 Hz, H-8), 6.20 (1H, d, *J* = 1.8 Hz, H-6), 5.35 (1H, d, *J* = 1.6 Hz, H-1″), 4.22 (1H, dd, *J* = 3.2, 1.6 Hz, H-2″), 3.75 (1H, dd, *J* = 9.2, 3.2 Hz, H-3″), 3.43 (1H, dd, *J* = 5.9, 9.6 Hz, H-5″), 3.34 (1H, dd, *J* = 5.9, 9.6 Hz, H-4″), 0.94 (3H, d, *J* = 5.6 Hz, CH3-6″). ^{13}C NMR (CD_3OD, 100 MHz, δ_C) 178.20 (C-4), 164.62 (C-7), 161.82 (C-5), 157.91 (C-2), 157.12 (C-9), 148.39 (C-4′), 145.04 (C-3′), 134.84 (C-3), 121.56 (C-1′), 121.44 (C-6′), 115.51 (C-5′), 114.95 (C-2′), 104.47 (C-10), 102.09 (C-1″), 98.44 (C-6), 93.32 (C-8), 71.85 (C-4″), 70.71 (C-2″), 70.62 (C-3″), 70.50 (C-5″), 16.10 (C-6″). HRESIMS: m/z 449.1079 $[M+H]^+$.

Compound 1 was a yellow amorphous powder. The IR spectrum showed the presence of the OH and carbonyl functional groups at 3,391 cm^{-1} and at 1656 cm^{-1}, respectively. C-H stretching vibrations appeared at 2,978 cm^{-1}, C=C stretching at 1,361 cm^{-1}, asymmetric C-O-C stretching at 1,171 cm^{-1}, and C-H bending at 839 cm^{-1}. The protons at positions C-6 and C-8 of ring A of the flavonol skeleton were predicted by the two aromatic hydrogen signals with 'meta coupling' at δ 6.34 ppm (1H, d, *J* = 1.6 Hz) and 6.17 (1H, d, *J* = 1.6 Hz) which appeared in

the 1H NMR spectra. Compound 1 was predicted to contain OH groups at C-5 and C-7 of ring A. The protons at positions C-2′, C-3′, C-5′, and C-6′ were assumed to be responsible for two signals with "ortho coupling" in ring B at δ 7.76 ppm (2H, dd, *J* = 8.8 Hz) and 6.92 ppm (2H, dd, *J* = 8.4 Hz). The compound was anticipated to be a flavonol rhamnoside based on the existence of an anomeric proton signal at δ 5.36 ppm (1H, d, *J* = 1.6 Hz) and the absence of a specific signal for olefinic hydrogen at C-3. A sugar moiety was present as evidenced by the formation of an anomeric carbon signal at 102.07 ppm in the ^{13}C NMR spectrum. The location of the sugar moiety was determined to be in the C-3 OH group based on the correlation between the anomeric proton signal (5.37 ppm) and the anomeric carbon signal (102.07 ppm) which were identified by analyzing the HMBC spectral data. The sugar moiety was identified as rhamnose by the methyl signal seen at 0.91 ppm (3H, s) in the 1H NMR spectrum and at 16.10 ppm in the ^{13}C NMR spectrum. The peak at m/z 455.0951 $[M+Na]^+$ was identified by the HRESIMS data as having the chemical formula $C_{21}H_{20}O_{10}$ (calculated for $C_{21}H_{20}O_{10}Na$, 455.0954 m/z). From the data, the isolated compound was identified as kaempferol-3-*O*-rhamnoside (Figure 1). We confirmed compound 1 to be kaempferol 3-*O*-rhamnoside by comparing the spectrum data of the isolated chemical with prior studies (27).

Compound 2 appeared as a yellow, amorphous powder. The spectrum data of compound 2 were similar to that of compound 1. The IR data showed that the absorption at 3,391, 2,932, 1,655, 1,359, 1,173, and 814 cm^{-1} were vibrations of the OH group, C-H stretching, the carbonyl functional group, the C=C olefin ring, C-O-C stretching, and C-H bending, respectively. Five aromatic proton signals at δ 7.32 ppm (1H, d, *J* = 2.0 Hz), 7.30 ppm (1H, dd, *J* = 8.0, 2.0 Hz), 6.91 ppm (1H, d, *J* = 8.4 Hz), 6.38 ppm (1H, d, *J* = 2.0 Hz), and 6.20 ppm (1H, d, *J* = 1.8 Hz) were observed in the 1H NMR spectra and were anticipated to be from the protons at C6, C8, C-2′, C-5′, and C6′. In ring A of the flavonol skeleton, two meta-coupled aromatic protons at δ 6.20 and 6.38 ppm (*J* = 2.0 Hz) indicated proton substitutions. Two aromatic proton signals with meta-coupling appeared at δ 7.32 ppm (d, *J* = 2.0 Hz) and 7.30 ppm (dd, *J* = 2.0 Hz), confirming three proton substitutions in ring B. The ortho coupling between the proton at δ 6.91 ppm and the proton at δ 7.30 ppm had a coupling constant of *J* = 8.0 Hz. The ^{13}C NMR spectrum contained 21 carbons, including 6 rhamnosyl carbon signals, (16.10, 102.09, 70.71, 70.62, 71.85, and 70.50 ppm). From the peak at m/z 449.1079 $[M+H]^+$ (calculated for $C_{21}H_{20}O_{11}H$, 449.1083 m/z), the chemical formula was determined to be $C_{21}H_{20}O_{11}$. We identified compound 2 as quercetin-3-*O*-rhamnoside (Figure 1) by comparing the spectrum data of the isolated compound with relevant literature (27).

In vitro analysis

Antioxidant activity of the test compounds was measured by ABTS assay. The results indicated that both compounds 1 and 2 showed an ability to scavenge ABTS radicals with IC_{50} values of 424.57±2.97 and 308.67±9.90 µM, respectively. Compound 2 scavenged ABTS radicals better than compound 1. For AChE

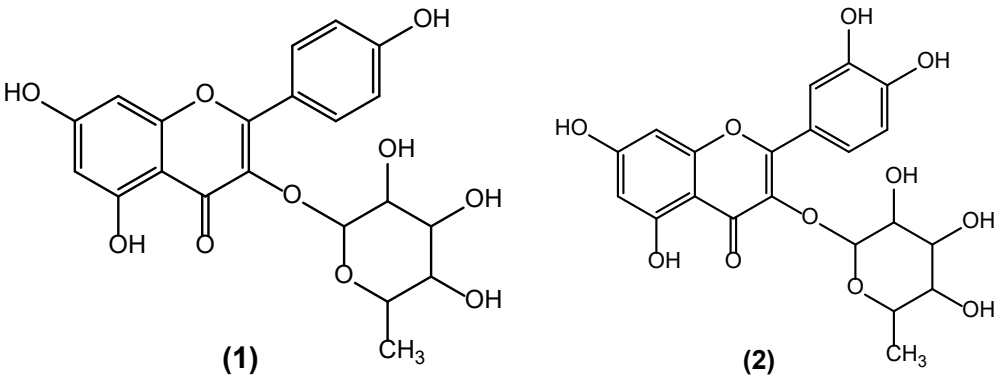

Figure 1. Structures of flavonoid rhamnosides: kaempferol-3-*O*- rhamnoside (compound 1) and quercetin-3-*O*-rhamnoside (compound 2).

inhibition, compound 1 showed an ability to inhibit AChE activity with IC_{50} 769.23±6.23 µM, while compound 2 could inhibit AChE function with an IC_{50} value of 520.64 ±5.94 µM. The investigation of the effect on Aβ aggregation showed that both compounds have an ability to inhibit Aβ aggregation with an IC_{50} values of 406.43±9.95 µM (compound 1) and 300.69 ±1.18 µM (compound 2). In summary, *in vitro* examination found that compound 2 showed better antioxidant activity as well as greater AChE and Aβ aggregation inhibition than compound 1. The results are presented in Table 1.

Flavonol compounds protect SH-SY5Y cells against H_2O_2-induced neurotoxicity

The neuroprotective effect against H_2O_2 toxicity of the flavonol compounds was determined in SH-SY5Y neuroblastoma cells. Before performing the neuroprotective assay, compounds 1 and 2 were tested for cytotoxicity against SHSY-5Y cells. The cells were treated with the test compounds at concentrations of 0.1, 1, 10, and 100 µM for 2 hours. The results showed that both test compounds were non-toxic to SHSY-5Y cells at concentrations up to 100 µM. Compounds 1 and 2 at the non-toxic concentrations of 0.1-100 µM were used in further neuroprotective effect investigation. In the neuroprotective assay, both compounds 1 and 2 showed neuroprotective effects against H_2O_2-induced neurotoxicity (Figure 2). Pretreatment of the cells with compound 1 at a concentration of 100 µM significantly reduced the cell viability loss induced by H_2O_2. Compound 2 greatly decreased the loss of cell viability induced by H_2O_2 at doses of 10 and 100 µM. The results obtained from the antioxidant assay indicate that both compounds exhibit antioxidant activity, indicating that the protective action against the H_2O_2 of compounds 1 and 2 might be enhanced by the antioxidant action.

Table 1. The activities related to AD of the flavonol compounds.

Test compounds	IC_{50} (µM)		
	Antioxidant	AChE inhibition	Anti-Aβ aggregation
Compound 1	424.57±2.97[a]	769.23±6.23[a]	406.43±9.95[a]
Compound 2	308.67±9.90[b]	520.64±5.94[b]	300.69±1.18[b]
Trolox	64.83±0.77[c]	ND	ND
Tacrine	ND	0.40±1.3[c]	ND
Curcumin	ND	ND	5.00±2.35[c]

Values expressed as mean ± SD (n = 3); [a,b,c] different letters in the same column are significantly different ($p < 0.05$).

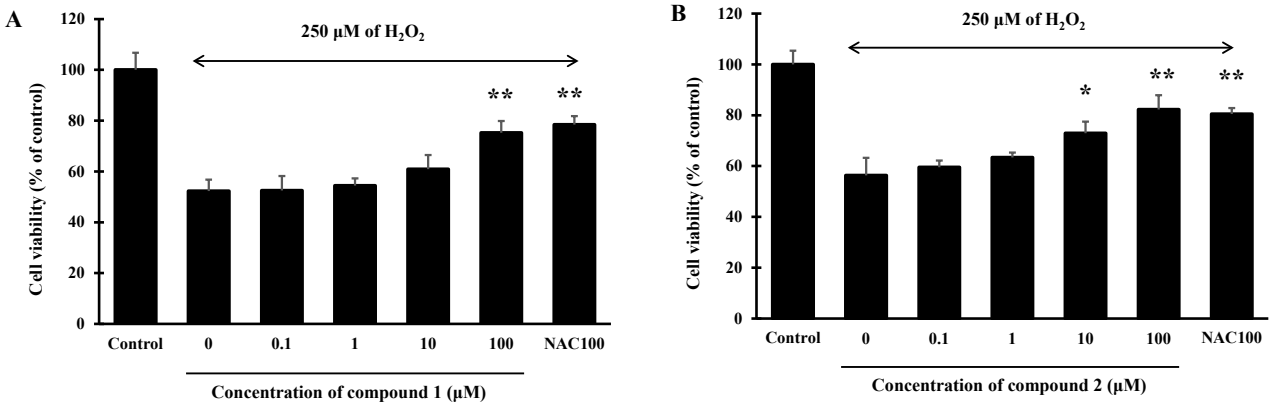

Figure 2. Effect of the flavonol compounds on H_2O_2-induced cell damage in SH-SY5Y cells: (A) compound 1; (B) compound 2. Data are means±SD (n=3) and $^{*}p < 0.05$, $^{**}p < 0.01$ compared to the H_2O_2-treated group

In-silico binding interaction studies

Molecular docking studies of AChE inhibition

The binding interactions between flavonol rhamnosides and AChE were examined to further define the underlying mechanism utilizing the Autodock 4.2.6 and Discovery studio programs. Compounds 1 and 2 bound to AChE with binding energy values of -11.65 and -14.40 KJ/mol, respectively. The compound 1 occupied in middle gorge of the AChE active site by locating ring B in the peripheral anionic site (PAS) region and the rhamnoside structure in the catalytic active site (CAS). Rings A and C, which are the core structure of flavonoids, interacted with Trp84 via π−π stacking. Ring B formed a π−π stacking interaction with Tyr334 in the PAS regions. The OH group at position 3 of rhamnoside interacted with Ser220 and His440 in the CAS via hydrogen bonding. The OH group at position 5 of ring A interacted with His440 in the CAS via a hydrogen bond. The binding modes and interaction diagrams of compound 1 bound to AChE are presented in Figure 3A. The orientation of compound 2 is the same as compound 1, with ring A located in CAS and ring B in regions of the AChE site. The benzene rings (A) and a heterocycle pyrene ring (C) formed hydrophobic π−π stacking interaction with Trp84 of PAS residue. The hydroxy group at position 3 of rhamnoside interacted with amino acid residues Ser220 and His440 via hydrogen bonding inside the active pocket of AChE. In addition, His440 showed hydrogen bonding with the hydroxy group of ring A at position 5. The OH group at position 3 of ring B exhibited hydrogen bonding interaction with Ser122. Figure 3B shows the binding interactions that occurred between compound 2 and surrounding amino acid residues that are located at the active sites.

Molecular docking studies of Aβ inhibition

Two flavonol rhamnosides were investigated for binding interactions between flavonol rhamnoside and $Aβ_{1-42}$. The interactions were determined using the Autodock 4.2.6 program. Compounds 1 and 2 bound to $Aβ_{1-42}$ with binding energy values of -6.54 and -8.36 KJ/mol, respectively. The core structure of compound 1 interacted with amino acid residue Val40 via π-stacked by hydrophobic interaction in the C-terminal hydrophobic region. In addition, the OH group at position 4 of ring B formed a hydrogen interaction with Ile41. Substitution with OH groups at positions 5 and 7 of ring B interacted with amino acid residue Leu17 in the central hydrophobic region. Thus, the core structure of compound 1 is located to the central hydrophobic core region and the C-terminal hydrophobic region of $Aβ_{1-42}$, which is responsible for promoting fibril formation and

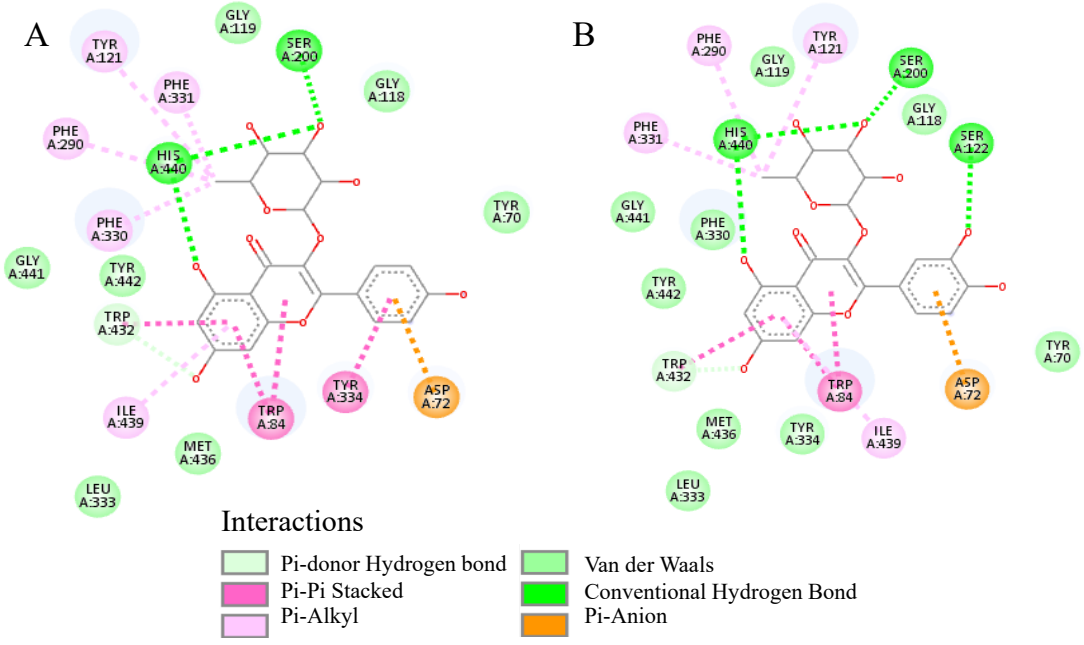

Figure 3. Binding interaction diagram of flavonol compounds: compound 1 (A), compound 2 (B) bound to AChE

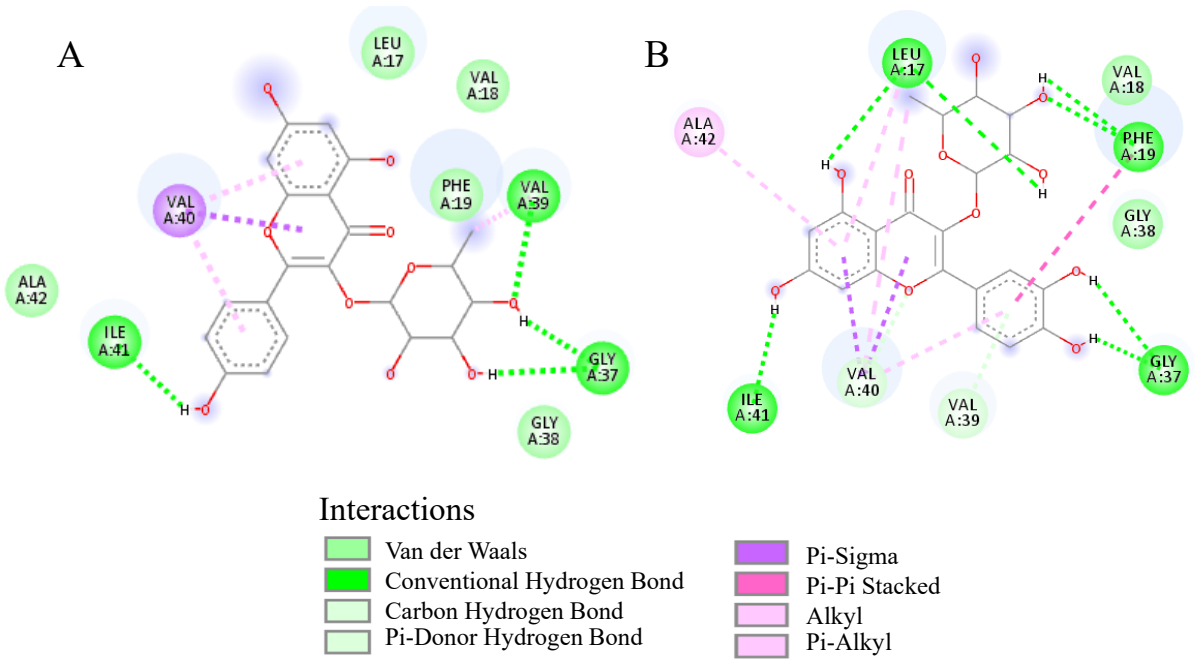

Figure 4. Binding interaction diagram of flavonol compounds: compound 1 (A), compound 2 (B) bound to $A\beta_{1-42}$

initiating nucleation. In addition, substitution with OH groups at positions 3 and 4 of rhamnoside interacted with amino acid residue Gly37 and Val39 via hydrogen bonding (Figure 4A). The binding orientation of compound 2 was the same as compound 1. The benzene rings (A) and a heterocycle pyrene ring (C) formed a hydrophobic π- sigma interaction with Val40 of the C-terminal hydrophobic region. The OH group at positions 5 and 7 of ring A interacted with Leu17 and Ile41 via hydrogen bonding. Ring B formed a π−π stacking interaction with Phe19. Amino acid residue Gly37 showed hydrogen bonding with the hydroxy group at positions 3 and 4 of ring B. The OH group at positions 2 and 3 of rhamnoside formed with Leu17 and Phe19, respectively, via hydrogen bonding in the central hydrophobic region (Figure 4B). These results indicate that these amino acids play a significant role in the networks of intra- and inter-molecular contacts that preserve the stability of fibrils through hydrogen bonding and hydrophobic interactions.

DISCUSSION

One of the direct causes of AD is oxidative stress. Overwhelming evidence suggests that oxidative stress is a factor in the development of AD and that it affects the brain tissue of patients. It is believed that oxidative stress, which is characterized by an imbalance in the creation of radical reactive oxygen species (ROS) and antioxidative defense, has a significant impact on age-related neurodegeneration and cognitive decline (28). Therefore, antioxidants might be useful for the prevention of oxidative stress in the AD brain. In this study, both flavonol compounds showed antioxidant activity in ABTS assay. The ability of compound 2 to scavenge ABTS radicals was higher than compound 1. These results revealed the importance of the OH group on position 3 of ring B of the flavonol skeleton as being important sites for scavenging free radicals. Normally, free hydroxyls on the flavonoid nucleus donate electrons, which results in the creation of less reactive aroxyl radicals (29). For this reason, it has been suggested that compound 2, which has two OH on ring B, is a stronger antioxidant than compound 1. Thus, it could be anticipated that the quantity of OH groups on ring B of the flavonol skeleton would affect the free radical scavenging ability. This is in accordance with previous research that found associations between the amounts of hydroxy groups on aromatic rings and their capacity to scavenge free radicals (30).

AD has been found to be associated with a decrease in the amount of acetylcholine in the brain, resulting in a cholinergic deficit. Acetylcholine is rapidly hydrolyzed by AChE at the cholinergic synapses, resulting in stopping

the transmission of nerve signals (31). Thus, it appears that inhibiting AChE function is an effective treatment approach to lessen, at least temporarily, the cognitive loss in AD. In the present study, the inhibitory activities of flavonol compounds against AChE were investigated by *in vitro* and molecular docking studies. In the *in vitro* study, both compounds showed an ability to inhibit acetylcholinesterase function. The degree of inhibition activity was found to vary depending on whether the structures of compound 2 provided stronger inhibition than compound 1. We confirmed that the OH group at the C-3 position in the structure of compound 2 increased AChE inhibitory activity and that it was essential for the occurrence of that activity. Similar results have been reported for quercetin and luteolin, with additional OH groups on the C-3 position of ring B showing activity higher than kaempferol and apigenin, respectively (32). According to the docking study, both flavonol rhamnosides concurrently occupy CAS and PAS of AChE. Interacting with His400 and Ser200 in CAS, the OH group of the rhamnoside structure plays a crucial role in the suppression of AChE activity. As a result, the flavonol rhamnoside attaches to the CAS of AChE and prevents ACh from being hydrolyzed. Moreover, the core structure of flavonoid could bind to the PAS via $\pi-\pi$ stacking with Tyr334 and Trp84, initiating the Aβ aggregation process.

The accumulation of toxic Aβ plaques in the brain is the key hallmark of AD pathogenesis. Therefore, the primary goal of numerous treatment approaches that are being developed or are undergoing clinical trials is to prevent or reduce the formation of Aβ plaques. $A\beta_{1-40}$ and $A\beta_{1-42}$ are the major elements of senile plaques (33, 34). According to several studies, $A\beta_{1-42}$ plays a significant role in the genesis of AD. According to previous research on transgenic mice and *in vitro* studies, $A\beta_{1-40}$ may produce amyloid plaques more slowly than $A\beta_{1-42}$ (35). Therefore, in order to evaluate the Aβ aggregation, we used $A\beta_{1-42}$. The cross-β structure of $A\beta_{1-42}$ fibrils consists of unstructured amino acid residues 1-17 at the N-termini, whereas amino acid residues 18-42 form the β-turn-β fold. There are two parallel β-turn regions, amino acid residues 17-21 and 29-35. These two β-strands are linked by a loop region where a salt bridge between Asp23 and Lys28 is created, supporting turn formation. The β-sheet structure is stabilized by two molecular interactions including that Phe19 packs against Gly38 and that Ala42 contacts the side chain of Met35. It has previously been determined that amino acid residues 17-21 in the central hydrophobic region and amino acid residues 39-42 in the C-terminal hydrophobic segment serve as the nucleation sites of Aβ aggregation. The steric zipper effect of these regions causes dimer formation and eventually greater aggregation. Interchain interactions are observed along with hydrogen bonds between the backbone of amino acid residues Val18-Val39, Asp23-Leu34, Lys28-Val36, Glu22-Met35, Val36-Ile41, and Phe20-Gly37. Additionally, it has been demonstrated that the addition of the amino acids Ile41 and Ala42 has a major impact on the development of AD. The production of paranuclei depends on amino acid Ile41, whereas the assembly of bigger oligomers requires Ala42 (36, 37). The central hydrophobic segment, the hydrophobic C-terminal, and the turn segment are vital areas of $A\beta_{1-42}$ that may enhance conformational shift, initiate nucleation, and encourage fibril formation. Compounds that have a potential to interact with these binding regions may be potent inhibitors of Aβ aggregation. In this study, both *in vitro* and *in-silico* methods were used to investigate the regulatory impact and mechanism of action of flavonol rhamnoside on $A\beta_{1-42}$ aggregation. In the *in vitro* study, we investigated the effects of two flavonol rhamnosides on the inhibition of Aβ aggregation using the ThT assay. The results showed that compound 2 could inhibit the aggregation of $A\beta_{1-42}$ more potently than compound 1. Compound 2 has many hydroxyls OH groups, which are crucial for inhibiting fibril growth by establishing hydrogen bonds through hydrophobic interactions between β-sheet structures and aromatic rings. By increasing the electron density in the aromatic rings, the hydroxyl OH group may improve the binding of compound 2 to the amino acid residue of β-sheet structures. The anti-amyloidogenic activity of the molecule increases with the number of OH groups

present in the structure (38). The results of the *in-silico* study showed the core structure of both compounds could form hydrophobic interactions with Val40 via π-stacked in the C-terminal hydrophobic region. For compound 1, substitution with OH group at position 4 of ring B formed a hydrogen bond only with Ile41, while compound 2 substitution with OH groups at positions 5 and 7 of ring A and at positions 3 and 4 of ring B enhanced hydrogen bonding with Leu17, Gly37 and Ile41. These amino acids play a significant role in the networks of intra- and intermolecular contacts that preserve the stability of fibrils through hydrogen bonding and hydrophobic interactions. The *in-silico* results indicate that the critical regions responsible for Aβ fibrillation and nucleation, the central hydrophobic segment and C-terminal hydrophobic area, as well as the residues at positions 41, may interact with flavonol rhamnoside to disrupt fibril stability.

Oxidative stress has been linked to AD, a neurodegenerative illness. An increase in the oxidation of brain lipids, carbohydrates, proteins, and DNA is characteristic of neurodegenerative disorders. Since the brain is a metabolically active organ, its levels of ROS are higher than those of other organs. The cell types most susceptible to free radical damage are neurons (39). Overproduction of ROS can result in cell death by damaging oxidative macromolecules. Oxidative stress has been linked to the onset and progression of neurodegenerative diseases, especially Alzheimer's disease (40). Therefore, reducing oxidative stress is one of the best ways to treat these diseases. Hydrogen peroxide (H_2O_2) acts as an inducer of oxidative stress damage by raising ROS levels and inducing cell death. H_2O_2 can also penetrate cell membranes and generate oxygen-derived free radicals. Thus, the Fenton reaction allows H_2O_2 to be transformed into hydroxyl radicals ($^{\cdot}OH$) in the presence of ferrous ions (Fe^{2+}) (41). For that reason, H_2O_2 was used to induce cell damage via oxidative stress. In this study, pretreatment of SH-SY5Y cells with compounds 1 and 2 greatly improved the survival of cells exposed to H_2O_2. The antioxidant abilities of both compounds could possibly explain their neuroprotective effects.

Overall, the results showed that two flavonol rhamnosides isolated from *M. ferrea* L. flower, kaempferol 3-*O*-rhamnoside and quercetin 3-O-rhamnoside, have multimode action related to the AD pathogenesis cascade, including antioxidants, anti-acetylcholinesterase, and anti-Aβ aggregation. In addition, both flavonol rhamnosides showed an ability to protect against neuronal cell damage induced by oxidative stress.

CONCLUSION

Two flavonoids isolated from *M. ferrea* L. flower, namely kaempferol-3-*O*-rhamnoside (1), quercetin-3-*O*-rhamnoside (2), were investigated for their activities involved with AD pathogenesis including antioxidant activity, AChE inhibition, anti-Aβ aggregation, and neuroprotection. Both compounds showed multifunctional activities targeting oxidation, AChE function and Aβ aggregation. The binding interactions between flavonol rhamnosides and AChE or $Aβ_{1-42}$ peptide were also examined in-silico to clarify the mechanism of action. The results demonstrated that both compounds could bind to AChE at both the CAS and the PAS, thus preventing the hydrolysis of ACh and Aβ aggregation. *In-silico* results revealed that both compounds might inhibit $Aβ_{1-42}$ aggregation by interacting with the residues of Ile41, the central hydrophobic core, and the C-terminal hydrophobic region of $Aβ_{1-42}$which are the important regions responsible for Aβ nucleation and fibrillation. Flavonoid rhamnosides were found to be multi-target agents that have the potential to prevent AD pathogenesis. Further studies to elucidate the mechanisms of action and the investigation in animal AD models, an important step in the search for new drug candidates, should be undertaken.

ACKNOWLEDGEMENTS

This reserch project is supported by Research and Graduate Studies, Khon kaen University, Thailand and BCG Economy and Sustainable Development Network through Center of Excellence Consortium under the Reinventing University System/visiting Professor Program 2023.

FUNDING

This research was funded by the Fundamental Fund of Khon Kaen University under the National Science, Research and Innovation Fund; Scholarship for Oversea Graduate Research, Khon Kaen University; the Research and Graduate Studies Program, Khon Kaen University; and Ubon Ratchathani University, Thailand.

CONFLICTS OF INTEREST

The authors declare no conflict of interest.

ADDITIONAL INFORMATION

Author contributions

Conceptualization, C.B., P.W., C.Y., O.M., N.N., Y.C., S.D., J.K. and S.A.; methodology, P.W., C.Y., and C.B.; formal analysis, P.W., K.P., C.Y., and C.B.; investigation, K.P., P.T., C.Y., O.M., P.W. and C.B.; resources, P.W. and C.B.; writing—original draft preparation, K.P., and C.B.; writing—review and editing, P.W. and C.B.; project administration, C.B. All authors have read and agreed to the published version of the manuscript.

REFERENCES

1. Alzheimer's Disease International. World Alzheimer Report 2019-Attitudes to dementia. London: Alzheimer's Disease International. 2019.
2. Alzheimer's Association. 2021 Alzheimer's disease facts and figures. Alzheimers Dement. 2021;17: 327-406.
3. Jia J, Wei C, Chen S, Li F, Tang Y, Qin W, et al. The cost of Alzheimer's disease in China and re–estimation of costs worldwide. Alzheimers Dement. 2018;14:483-91.
4. Hardy JA, Higgins GA. Alzheimer's disease: The amyloid cascade hypothesis. Science. 1992;256: 184-5.
5. Naseri NN, Wang H, Guo J, Sharma M, Luo W. The complexity of tau in Alzheimer's disease. Neurosci Lett. 2019;705:183-94.
6. Yoo JH, Valdovinos MG, Williams DC. Relevance of donepezil in enhancing learning and memory in special populations: A Review of the literature. J Autism Dev Disord. 2007;37:1883–901.
7. Scrivo R, Vasile M, Bartosiewicz I, Valesini G. Inflammation as "common soil" of the multifactorial diseases. Autoimmun Rev. 2011;10:369-74.
8. Praticò D. Evidence of oxidative stress in Alzheimer's disease brain and antioxidant therapy: lights and shadows. Ann N Y Acad Sci. 2008:1147:70-8
9. Rosini M, Simoni E, Bartolini M, Cavalli A, Ceccarini L, Pascu N, et al. Inhibition of acetylcholinesterase, β-Amyloid aggregation, and NMDA receptors in Alzheimer's disease: a promising direction for the multi-target-directed ligands gold rush. J Med Chem. 2008;51:4381–4.
10. Švecová M, Ulbrich P, Dendisová M, Matějka P. SERS study of riboflavin on green-synthesized silver nanoparticles prepared by reduction using different flavonoids: What is the role of flavonoid used? Spectrochim Acta A Mol Biomol Spectrosc. 2018;195:236-45.
11. Bowles D, Lim EK, Poppenberger B, Vaistij FE. Glycosyltransferases of lipophilic small molecules. Annu Rev Plant Biol. 2006;57:567-97.
12. Tahara S. A journey of twenty-five years through the ecological biochemistry of flavonoids. Biosci Biotechnol Biochem. 2007;71:1387-404.
13. Li J, Sun M, Cui X, Li C. Protective effects of flavonoids against Alzheimer's disease: pathological hypothesis, potential targets, and structure–activity relationship. Int J Mol Sci. 2022;23:10020. PubMed PMID: 36077418
14. Nandy S, Tiwari P. Screening of anti-inflammatory activity of Mesua ferrea Linn flower. Int J Biomed Res. 2012;3:245-52.
15. Garg S, Sharma K, Ranjan R, Attri P, Mishra P. In vivo antioxidant activity and hepatoprotective effects of methanolic extract of *Mesua ferrea* linn. Int J Pharmtech Res. 2009;1:1692-6.
16. Plekratoke K, Boonyarat C, Monthakantirat O, Nualkaew N, Wangboonskul J, Awale S, et al. The effect of ethanol extract from Mesua ferrea Linn flower on Alzheimer's disease and its underlying mechanism. Curr Issues Mol Biol. 2023;45:4063-79.
17. Manse Y, Sakamoto Y, Miyachi T, Nire M, Hashimoto Y, Chaipech S, et al. Antiallergic properties of biflavonoids isolated from the flowers of *Mesua ferrea* Linn. Separations. 2022;9:127.
18. Diantini A, Subarnas A, Lestari K, Halimah E, Susilawati Y, Supriyatna, et al. Kaempferol-3-O-rhamnoside isolated from the leaves of Schima wallichii Korth. inhibits MCF-7 breast cancer cell proliferation through activation of the caspase cascade pathway. Oncol Lett. 2012;3:1069-72.
19. Rodríguez P, González-Mujica F, Bermúdez J, Hasegawa M. Inhibition of glucose intestinal absorption by kaempferol 3-O-α-rhamnoside purified from Bauhinia megalandra leaves. Fitoterapia. 2010;81:1220-3.
20. Mehrbod P, Abdalla MA, Fotouhi F, Heidarzadeh M, Aro AO, Eloff JN, et al. Immunomodulatory properties of quercetin-3-O-α-L-rhamnopyranoside from Rapanea melanophloeos against influenza a virus. BMC Complement Altern Med. 2018;18:184. PubMed PMID: 29903008
21. Rajurkar N, Hande S. Estimation of phytochemical content and antioxidant activity of some se-

lected traditional Indian medicinal plants. Indian J Pharm Sci. 2011;73:146-51.
22. Ellman GL, Courtney KD, Andres V, Featherstone RM. A new and rapid colorimetric determination of acetylcholinesterase activity. Biochem Pharmacol. 1961;7:88-95.
23. Takomthong P, Waiwut P, Yenjai C, Sripanidkulchai B, Reubroycharoen P, Lai R, et al. Structure–activity analysis and molecular docking studies of coumarins from Toddalia asiatica as multifunctional agents for Alzheimer's disease. Biomedicines. 2020;8:107. PubMed PMID: 32370238
24. de Medeiros LM, De Bastiani MA, Rico EP, Schonhofen P, Pfaffenseller B, Wollenhaupt-Aguiar B, et al. Cholinergic differentiation of human neuroblastoma SH-SY5Y cell line and its potential use as an *In vitro* model for Alzheimer's disease studies. Mol Neurobiol. 2019;56:7355-67.
25. Chheng C, Waiwut P, Plekratoke K, Chulikhit Y, Daodee S, Monthakantirat O, et al. Multitarget activities of kleeb bua daeng, a Thai traditional herbal formula, against Alzheimer's disease. Pharmaceuticals. 2020;13:79. PubMed PMID: 32344916
26. Takomthong P, Waiwut P, Yenjai C, Sombatsri A, Reubroycharoen P, Lei L, et al. Multi-target actions of acridones from atalantia monophylla towards Alzheimer's pathogenesis and their pharmacokinetic properties. Pharmaceuticals. 2021; 14:888. PubMed PMID: 34577588
27. Utari F, Itam A, Syafrizayanti S, Hasvini Putri W, Ninomiya. Isolation of flavonol rhamnosides from Pometia pinnata leaves and investigation of α-glucosidase inhibitory activity of flavonol derivatives. J App Pharm Sci. 2019;9:53-65.
28. Gella A, Durany N. Oxidative stress in Alzheimer disease. Cell Adh Migr. 2009;3:88–93.
29. Crespo I, García-Mediavilla MV, Gutiérrez B, Sánchez-Campos S, Tuñón MJ, González-Gallego J. A comparison of the effects of kaempferol and quercetin on cytokine-induced pro-inflammatory status of cultured human endothelial cells. Br J Nutr. 2008;100:968-76.
30. Vajragupta O, Toasaksiri S, Boonyarat C, Wongkrajang Y, Peungvicha P, Watanabe H, et al. Chroman amide and nicotinyl amide derivatives: Inhibition of lipid peroxidation and protection against head trauma. Free Radic Res. 2000;32:145-55.
31. Hasselmo ME. The role of acetylcholine in learning and memory. Curr Opin Neurobiol. 2006;16:710-5.
32. Xie H, Wang JR, Yau LF, Liu Y, Liu L, Han QB, et al. Catechins and procyanidins of ginkgo biloba show potent activities towards the inhibition of β-amyloid peptide aggregation and destabilization of preformed fibrils. Molecules. 2014;19:5119-34.
33. Murphy MP, LeVine H. Alzheimer's disease and the amyloid-β peptide. J Alzheimers Dis. 2010;19:311-23.
34. Chen G fang, Xu T hai, Yan Y, Zhou Y ren, Jiang Y, Melcher K, et al. Amyloid beta: structure, biology and structure-based therapeutic development. Acta Pharmacol Sin. 2017;38:1205-35.
35. Gu L, Guo Z. Alzheimer's Aβ42 and Aβ40 peptides form interlaced amyloid fibrils. J Neurochem. 2013; 126:305-11.
36. Bitan G, Kirkitadze MD, Lomakin A, Vollers SS, Benedek GB, Teplow DB. Amyloid β-protein (Aβ) assembly: Aβ40 and Aβ42 oligomerize through distinct pathways. Proc Natl Acad Sci. 2003;100: 330-5.
37. Urbanc B, Cruz L, Yun S, Buldyrev SV, Bitan G, Teplow DB, et al. In silico study of amyloid β-protein folding and oligomerization. Proc Natl Acad Sci. 2004;101:17345–50.
38. Jiménez-Aliaga K, Bermejo-Bescós P, Benedí J, Martín-Aragón S. Quercetin and rutin exhibit antiamyloidogenic and fibril-disaggregating effects *in vitro* and potent antioxidant activity in APPswe cells. Life Sci. 2011;89:939-45.
39. Gilgun-Sherki Y, Melamed E, Offen D. Oxidative stress induced-neurodegenerative diseases: the need for antioxidants that penetrate the blood brain barrier. Neuropharmacology. 2001;40:959-75.
40. Kim GH, Kim JE, Rhie SJ, Yoon S. The role of oxidative stress in neurodegenerative diseases. Exp Neurobiol. 2015;24:325-40.
41. Ofoedu CE, You L, Osuji CM, Iwouno JO, Kabuo NO, Ojukwu M, et al. Hydrogen Peroxide Effects on Natural-Sourced Polysacchrides: Free Radical Formation/Production, Degradation Process, and Reaction Mechanism—A Critical Synopsis. Foods. 2021;10:699. PubMed PMID: 33806060